Faraday Discussions

Cite this: DOI: 10.1039/c8fd00101d

PAPER

View Article Online
View Journal

Priming effects in the crystallization of the phase change compound GeTe from atomistic simulations

Silvia Gabardi, [a] Gabriele G. Sosso, [b] Joerg Behler [c] and Marco Bernasconi *[a]

Received 27th May 2018, Accepted 3rd August 2018
DOI: 10.1039/c8fd00101d

Strategies to reduce the incubation time for crystal nucleation and thus the stochasticity of the set process are of relevance for the operation of phase change memories in ultra-scaled geometries. With these premises, in this work we investigate the crystallization kinetics of the phase change compound GeTe. We have performed large scale molecular dynamics simulations using an interatomic potential, generated previously from a neural network fitting of a database of *ab initio* energies. We have addressed the crystallization of models of amorphous GeTe annealed at different temperatures above the glass transition. The results on the distribution of subcritical nuclei and on the crystal growth velocity of postcritical ones are compared with our previous simulations of the supercooled liquid quenched from the melt. We find that a large population of subcritical nuclei can form at the lower temperatures where the nucleation rate is large. This population partially survives upon fast annealing, which leads to a dramatic reduction of the incubation time at high temperatures where the crystal growth velocity is maximal. This priming effect could be exploited to enhance the speed of the set process in phase change memories.

1 Introduction

Chalcogenide alloys are exploited in non-volatile phase change memories (PCM) thanks to their ability to undergo a fast and reversible transformation between the crystalline and amorphous phases upon Joule heating.[1–6] In PCMs the crystallization process of the amorphous phase takes place on the time scale of 10–100 ns at temperature in between the glass transition temperature T_g and the melting

[a]*Department of Materials Science, University of Milano-Bicocca, Via R. Cozzi 55, I-20125 Milano, Italy. E-mail: marco.bernasconi@unimib.it*

[b]*Department of Chemistry and Centre for Scientific Computing, University of Warwick, Gibbet Hill Road, Coventry CV4 7AL, UK*

[c]*Universität Göttingen, Institut für Physikalische Chemie, Theoretische Chemie, Tammannstr. 6, 37077 Göttingen, Germany*

temperature T_m. A detailed microscopic understanding of this process that sets the writing speed of the memory is thus of great practical relevance.

In recent years, information on the crystallization process at the operation conditions of the devices has been gained from ultra-fast differential scanning calorimetry (DSC) of the two prototypical phase change compounds for PCMs, $Ge_2Sb_2Te_5$ (GST) and GeTe.[7–10] The experimental DSC data suggest that the high crystallization speed originates from the high fragility of the supercooled liquid, which allows for a high atomic mobility (low viscosity) at temperatures substantially lower than T_m at which the thermodynamic driving force for crystallization is also large. Electrical measurement techniques have confirmed the non-Arrhenius crystallization kinetics typical of a fragile liquid for GST confined in a memory cell.[11–13] Time resolved transmission electron microscopy has also been used to investigate the crystallization kinetics of GeTe close to T_m.[14]

Recent analysis of the DSC data of GST by means of classical nucleation theory (CNT)[15] shows that the homogeneous nucleation rate is maximal at 0.59 T_m while the maximal crystal growth velocity (few m s^{-1}) occurs at about 0.76 T_m. In a transient nucleation regime the overall crystallization rate depends on the population of subcritical nuclei generated during the annealing process of the amorphous phase from T_g to the temperature of maximal crystal growth velocity. A large population of subcritical nuclei reduces the incubation time needed for the formation of a postcritical nucleus. The shorter incubation time of melt-quenched GST compared to the as-deposited amorphous phase is indeed ascribed to the presence of quenched-in crystallites in the melt quenched phase.[16]

The population of subcritical nuclei can be enlarged also by pre-annealing the system, as demonstrated in GST by Loke *et al.*[17] who reported a dramatic reduction of the crystallization time from 5 ns to 0.5 ns upon application of a steady low voltage before the application of the set pulse. The generation of such subcritical crystallites is a priming effect that has been recently analyzed by Orava and Greer[15] within CNT. In this latter work, it has been shown that the equilibrium population of subcritical nuclei increases with temperature up to about 0.55 T_m and then it decreases, which explains the priming effect observed experimentally and its fading once the temperature is allowed to decrease before the set pulse is applied.[15]

The microscopic process of nucleation and growth in $Ge_2Sb_2Te_5$ has also been addressed by molecular dynamics (MD) simulations based on density functional theory (DFT).[18–20] Different crystallization conditions have been explored: either the homogeneous nucleation in the annealed amorphous phase or in the supercooled liquid, the growth of a supercritical nucleus introduced in an amorphous matrix by different means, or the crystallization from a planar amorphous/crystalline interface.[18–20] A very recent work has also reported a dependence of the incubation time for crystallization on the preparation conditions of small amorphous models (108-atom) of $Ge_2Sb_2Te_5$. Models generated by quenching from the melt in about 1.5 ns show shorter incubation time than fast-quenched models due to the presence of a larger population of crystalline seeds, albeit they have been quantified just by the number of four-membered rings typical of the crystalline phase.[21] The priming effect resulting from pre-annealing amorphous $Ge_2Sb_2Te_5$ at 420 K (just above T_g) has been directly simulated by DFT-MD in ref. 17 where it has been shown that the annealing induces a prestructural ordering in the amorphous phase that

facilitates the formation of critical nuclei during further annealing (the set pulse) at higher temperatures. Preordering effects facilitating crystal nucleation were also observed in other DFT simulations (460-atom cell) of $Ge_2Sb_2Te_5$.[22] In this latter work, an easier crystallization was found in an amorphous model that experienced a history of order.

Recently, DFT calculations also suggested a different strategy to reduce the incubation time by suitably alloying the Sb_2Te_3 compound with Scandium. The stronger Sc–Te bonds (with respect to the Ge–Te and Sb–Te bonds in GST) are responsible for the long lifetime of the Sc–Te square rings that act as crystalline precursors facilitating the formation of postcritical nuclei.[23]

In the case of the GeTe compound, large scale MD simulations of the crystallization process have been performed using an interatomic potential generated by fitting a large DFT database with a neural network (NN) scheme.[24–26] Simulations with the NN potential and cells containing up to 32 000 atoms allowed us to study of the homogeneous crystallization[24] and the crystal growth at the liquid–crystal interface in the bulk[25] and in nanowires.[27] The simulations provided a quantitative evaluation of the crystal growth velocity as a function of temperature that validated the application of classical theory for the crystal growth velocity.[28] These simulations of GeTe, however, always considered the crystallization of the supercooled liquid obtained by quenching from the melt. In view of the arguments discussed above on priming effects, it would be interesting to investigate whether differences in the crystallization speed could be found by heating the amorphous phase above T_g with respect to the results obtained at the same temperature in our previous work for the supercooled liquid generated by quenching from T_m.

To this end, we here report on the NN simulations of the crystallization process of 4096-atom models of amorphous GeTe (a-GeTe) annealed at different temperatures above T_g. Two amorphous models were considered as generated by quenching from T_m in either 100 ps or 3 ns. The distribution of nuclei formed at different temperatures and the crystal growth velocity of overcritical nuclei during the annealing process are analyzed and the results are compared with our previous simulations of the crystallization in the supercooled liquid phase.

2 Computational details

The molecular dynamics simulations were performed using the interatomic potential for GeTe generated in ref. 26 by fitting a large DFT database by means of the neural network method introduced by Behler and Parrinello.[29] The database consists of the DFT total energy of about 30 000 configurations of 64-, 96- and 128-atom cells computed with the Perdew–Burke–Ernzerhof exchange and correlation functional[30] and norm conserving pseudopotential as implemented in the Quantum-ESPRESSO suite of programs.[31] The reliability of the potential was validated in our previous works on the study of the properties of liquid, amorphous, and crystalline GeTe.[24–27,32–36] The theoretical melting temperature of $T_m = 1001$ K, obtained in ref. 32 from thermodynamic integration (or $T_m = 1023$ K with a slightly different setting), is close to the experimental value of 998 K.[37] The MD simulations were performed with the NN code RuNNer[38] using the DL_Poly code as the MD driver.[39] A stochastic thermostat was used to perform constant temperature simulations with a time step of 2 fs.[40]

The amorphous models in cubic 4096-atom supercells were generated by quenching from 1000 K to 300 K in either 100 ps (fast-quenched model) or 3 ns (slow-quenched model) at the fixed density of 0.0355 atoms per $Å^3$, which is very close to the experimental one of 0.03327 atoms per $Å^3$ for the amorphous phase.[41]

The evolution of temperature with time during the quenching protocol in the slow and fast-quenched models is reported in Fig. 1. In the slow quenching protocol the quenching rate in the temperature range 500–700 K is higher than at other temperatures to prevent crystallization (see Fig. 1).

The amorphous models were then heated in nine steps at temperatures of 500, 525, 550, 575, 600, 625, 650, 675, and 700 K. At each temperature the system was equilibrated for 25 ps before increasing the temperature by 25 K in another 25 ps. The overall annealing time from 300 K to 700 K is thus 9×50 ps $= 450$ ps. At each step the system is then simulated at constant temperature for about 1.4 ns to study the crystallization kinetics.

To identify the crystalline nuclei we used the local order parameter $Q_6(i)$,[42,43] defined for each atom i as

$$Q_6(i) = \sum_{j=1}^{N_b(i)} \frac{\sum_{m=-6}^{6} q_{6m}(i) q_{6m}^*(j)}{\left(\sum_{m=-6}^{6} |q_{6m}(i)|^2\right)^{1/2} \left(\sum_{m=-6}^{6} |q_{6m}(j)|^2\right)^{1/2}}, \quad \text{with}$$

$$q_{6m}(i) = \frac{1}{N_b(i)} \sum_{j=1}^{N_b(i)} Y_{6m}(\hat{\mathbf{r}}_{ij}), \tag{1}$$

where $Y_{6m}(\hat{\boldsymbol{r}}_{ij})$ are the spherical harmonics of the polar angles defined by the versor $\hat{\boldsymbol{r}}_{ij}$, which links atoms i and j. The index j runs over the $N_b(i)$ neighboring

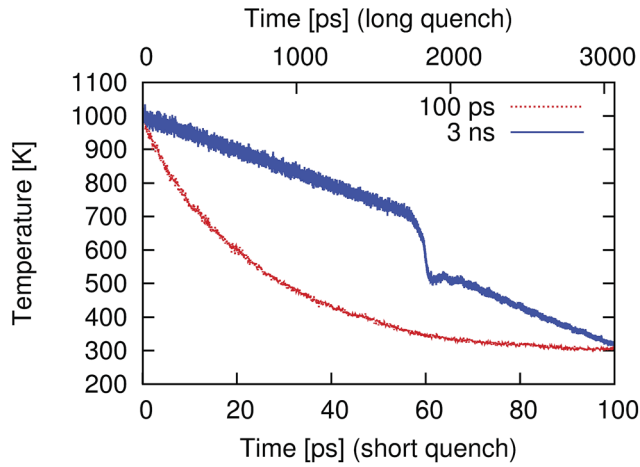

Fig. 1 Temperature as a function of time for the slow (upper curve) and fast (lower curve) quenching protocols used for the generation of the two a-GeTe models. The quenching rate in the temperature range 500–700 K is higher to prevent crystallization.

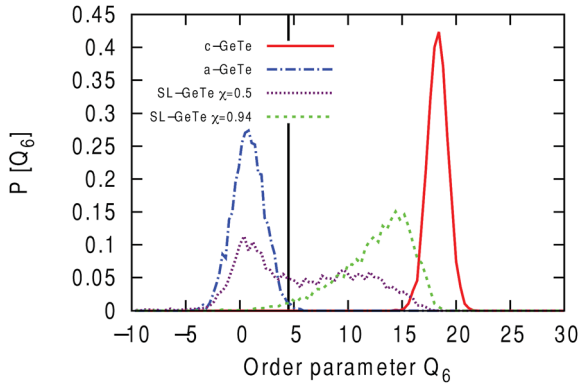

Fig. 2 Distribution of the order parameter for crystallinity Q_6 for a snapshot of the crystalline and amorphous models (4096-atom) in 300 K simulations at their theoretical equilibrium densities and two snapshots of the simulation at 675 K in which only a fraction ($\chi = 0.5$ and $\chi = 0.94$) of the atoms is crystallized.

atoms, which include the third coordination shell of crystalline GeTe at its theoretical equilibrium density. In our previous work[24] we showed that this order parameter is suitable to define an atom as crystalline when $Q_6 > 4.5$. Two crystalline atoms are considered connected up to a cutoff distance of 3.6 Å. These choices ensure that atoms at the interface between the nuclei and the disordered phase are also considered as crystalline. The distribution of the local order parameter for crystallinity Q_6 is shown in Fig. 2 for the amorphous and crystalline phases at 300 K and for two snapshots of the simulation at 675 K in which only a fraction of the atoms is crystallized. The analogous parameter Q_4 was also used in subsequent simulations.[25] We use the Q_6 parameter for the sake of comparison with the results of ref. 24 on the liquid phase supercooled from the melt where the Q_6 parameter was also used.

3 Results

Before discussing the simulations of the annealed amorphous phase, we briefly summarize our previous results on the crystallization of the supercooled liquid quenched from T_m.[24] We observed two different regimes in our simulations with 4096-atom cells. At temperatures below 600 K several nuclei appeared on the time scale of few hundreds of ps, while at temperatures in the range 600–675 K a single overcritical nucleus appeared after an incubation time up to 350 ps long. Above 675 K, we did not observe crystallization over 2 ns due to the decrease of the nucleation rate of overcritical nuclei approaching T_m. We then quantified the radius R of the growing nuclei as $R = (3V/4\pi)^{1/3}$ where V is the volume of the single crystallite defined by assigning the volume per atom of the bulk crystalline phase (β-GeTe) to each crystalline atom in the nucleus. The use of the Voronoi polyhedra actually gave very similar results for the crystallite volume. The crystal growth velocity u of each nucleus was then obtained as $u = dR/dt$ where t is the time. A clear linear growth of R with time was observed for the growing nuclei until different nuclei start to interact with each other (at temperatures below 600 K) slowing down the crystallization process.

Turning now to the crystallization of the annealed amorphous model, we consider first the fast-quenched model generated by quenching from the melt in 100 ps. In Fig. 3 we report the evolution with time of the total number of crystalline atoms at different temperatures.

Some differences can be outlined between the results obtained here and those reported in ref. 24 on the supercooled liquid (see Fig. 1a in ref. 24). In contrast with what was observed in the supercooled liquid quenched from the melt, at temperatures above 550 K we do not see here an incubation time and the fraction of crystalline atoms starts to increase with a clear slope from the very beginning of the simulations (zero time in Fig. 3). After a fast growth in the number of crystalline atoms, the crystallization slows down once only about half of the simulation cell is crystallized. On the contrary, in the simulation of the supercooled liquid in ref. 24, nearly the whole cell (4096-atom large as well) crystallized on the time scale of 1.5 ns was explored here. These differences originate from the fact that in the annealing of a-GeTe a large population of subcritical nuclei is generated at lower temperatures (500–600 K) in the short time span of the heating process from one step to the next (50 ps). This non-equilibrium population of subcritical nuclei facilitates the formation of more than one overcritical nucleus at higher temperatures. This leads to a reduction or even disappearance of the

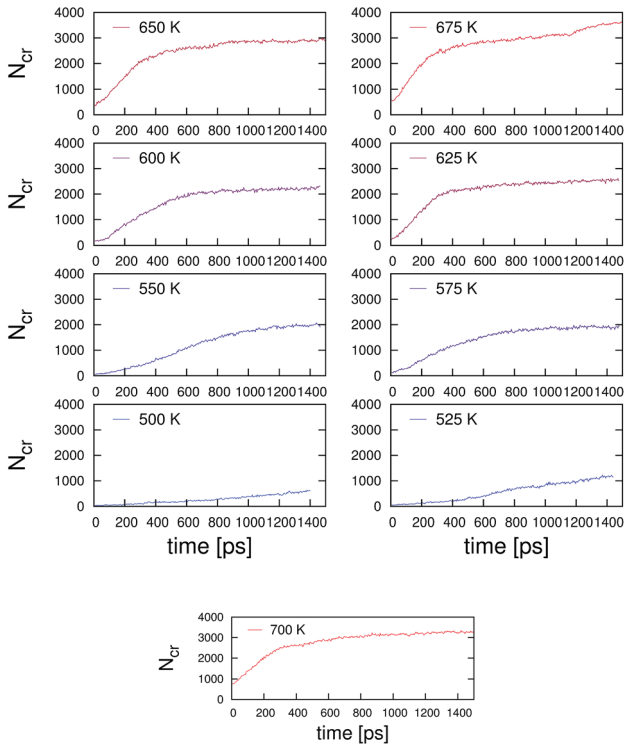

Fig. 3 Evolution with time of the number of crystalline atoms N_{cr} at different temperatures during the crystallization of the fast-quenched model (4096-atom) of a-GeTe (see text). The model is heated from 300 K to 700 K in nine steps lasting 50 ps each. The system is then monitored for 1.4 ns at constant temperature at each step of the heating process.

incubation time, but once the growing overcritical nuclei start to interact with each other the crystallization speed decreases. In fact, the atoms at the interface between nuclei with different crystallographic orientations take more time to order and to form a crystalline grain boundary. Coarsening of the different crystallites was also observed. On the contrary, in the supercooled liquid of ref. 24 subcritical nuclei were very few and the stochastic formation of a single large overcritical nucleus required an incubation time. On the other hand, the presence of a single growing crystalline nucleus allowed for the crystallization of nearly the whole simulation cell. At 700 K, no crystallization is observed in the supercooled liquid because an overcritical nucleus was not formed on the time scale of 1 ns, while crystallization is still observed in the annealed a-GeTe because of the persistence of subcritical nuclei formed at lower temperatures.

The population of the subcritical nuclei at the different temperatures and at different times for the annealed a-GeTe (fast-quenched model) is shown in Fig. 4. The number of crystalline nuclei containing more than 8 atoms (panel a) or more than 29 atoms (panel b) is shown. At lower temperatures an incubation time is still present to observe the formation of a nucleus larger than 29 atoms, but at and above 600 K a large fraction of larger nuclei (>29 atoms) are present at the very beginning of the simulation. They are formed during the annealing process (50 ps per step) and they survive at the higher temperatures.

This is a sort of priming effect: subcritical nuclei that form more easily at lower temperatures (here at and below 625 K) are brought to high temperatures where crystal growth velocity is higher. This effect is more evident by considering the population of smaller nuclei (>8 atoms) in Fig. 4a. The number of crystalline nuclei increases very fast in the temperature range 575–600 K and they survive in part during the annealing at the higher temperatures. Then their number

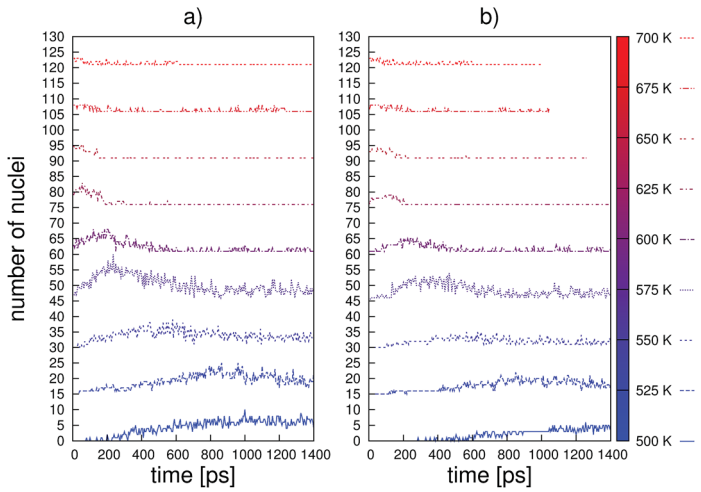

Fig. 4 The number of crystalline nuclei containing (a) more than 8 atoms or (b) more than 29 atoms as a function of time in constant temperature simulations of the fast-quenched model of a-GeTe. The evolution in time of the population of nuclei is reported at different temperatures. The curves corresponding to the different temperatures are shifted by 15 units along the ordinate axis.

decreases with time either because they coalesce forming larger nuclei or because they disappear. Still their presence is sufficient to allow for the formation of more than one overcritical nucleus with no incubation time. Snapshots of the crystalline nuclei at the beginning of the simulations at the different temperatures during the annealing process is shown in Fig. 5. Subcritical nuclei formed at lower temperatures survive during the heating process and continue growing leading to supercritical nuclei at higher temperatures in the range 650–675 K.

In Fig. 6 we report the evolution with time of the radius R of different nuclei at different temperatures from which we can compute the crystal growth velocity $u = \mathrm{d}R/\mathrm{d}t$. Since several nuclei are present, they interact with each other giving rise to a spread in the crystal growth velocities. The maximum velocity at each temperature, which corresponds to the nucleus interacting less with the others, is compared in Table 1 with the results of ref. 24 on the crystallization of the supercooled liquid quenched from T_m. The crystal growth velocities are very similar for the annealed amorphous phase and for the supercooled liquid up to 625 K, albeit slightly lower in the former one for most of the temperatures. This is consistent with the lower diffusion coefficient D computed for the overheated amorphous phase in our previous work.[44] We remark that the lower value of D in the annealed a-GeTe is also resulting in part from the presence of the population

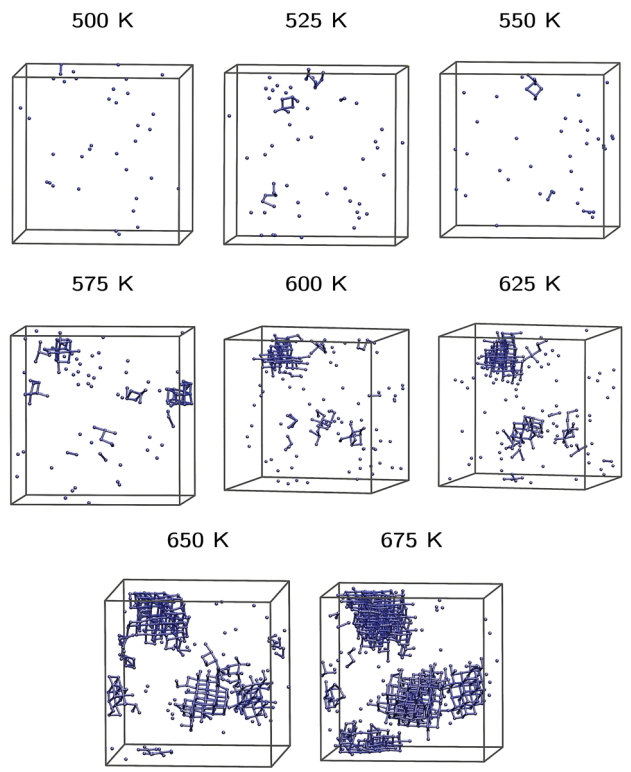

Fig. 5 Snapshots of the crystalline nuclei at the beginning of the simulations at different temperatures during the annealing process. Only crystalline atoms according to the value of the order parameter Q_6 (see text) are shown.

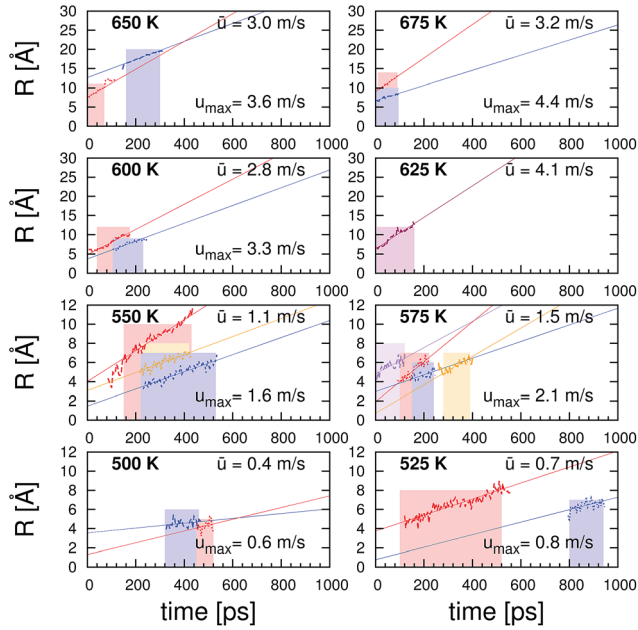

Fig. 6 Evolution with time of the radius R of different crystalline nuclei at different temperatures. The shadowed area indicates the time span over which the radius grows linearly with time before interactions with other nuclei slow down the crystallization process or it gives rise to coalescence or coarsening. The value of u_{max} refers to the maximum velocity recorded at the given temperature while u is the value averaged over the different nuclei.

of less mobile subcritical nuclei during the annealing process as evidenced here. At higher temperatures the crystal growth velocity obtained here for a-GeTe is sizably lower because the crystallites are already sufficiently large and numerous to interact with each other, slowing down the crystallization.

As a word of caution, we remark that the maximum crystal growth velocity in our simulations is overestimated with respect to experiments. A theoretical maximum crystal growth velocity of about 7.5 m s^{-1} was obtained in ref. 27 from

Table 1 Crystal growth velocity at different temperatures for the annealed a-GeTe model simulated here (fast quenched from the melt) and for the liquid supercooled below T_m of ref. 24. The maximum velocity is reported for annealed a-GeTe (see text and Fig. 6)

Temperature (K)	Amorphous annealed (this work), u (m s^{-1})	Liquid supercooled (ref. 24), u (m s^{-1})
500	0.6	0.45 ± 0.3
525	0.8	0.75 ± 0.2
550	1.6	1.9 ± 0.5
575	2.1	2.2 ± 0.3
600	3.3	3.5 ± 0.4
625	4.1	4.7
650	3.6	5.1
675	4.4	6.2

the simulation of the crystal growth at a planar crystal/liquid interface, while a maximum crystal growth velocity of 3.3 m s^{-1} or 3.5 m s^{-1} was measured by time-resolved electron diffraction[14] or by ultra-fast DSC.[10] This can be ascribed to a theoretical overestimation of the atomic mobility as emerged from the comparison of the viscosity computed by NN simulations[32] with recent experimental data for the supercooled liquid close to T_m.[45] It was actually shown that the mobility (viscosity) in the DFT simulations of the supercooled liquid could be reduced (increased) and brought to a better agreement with experiments using an exchange and correlation functional that includes van der Waals interactions (DFT-D2)[46] which are lacking in the DFT-PBE framework used in the generation of the NN potential. The overestimation of the atomic mobility can also lead to an overestimation of the priming effects observed here, as a higher atomic mobility also implies a short incubation time within CNT.[15,47]

We repeated the analysis of the crystallization kinetics for a second a-GeTe model generated by quenching from the melt at a much lower pace corresponding to an overall quenching time from 1000 K to 300 K of about 3.0 ns. The structural properties of the slow-quenched model was analyzed in our previous work.[49] The partial pair correlation functions are very similar for the fast- and slow-quenched models as shown in Fig. 7; the same is true for the bond angle distribution function and the distribution of the partial coordination numbers as discussed in ref. 49. The distribution of ring lengths computed according to ref. 50 and shown in Fig. 8 is also similar in the slow- and fast-quenched models.

Still, in the slow-quenched model there is a sizable fraction of small subcritical nuclei quenched-in at 300 K. They are evident in Fig. 9 which reports the evolution with time of crystalline nuclei (>8 atoms) in the slow-quenched model at different temperatures. The population of the nuclei at the beginning of the simulation at the lowest temperature of 500 K is close to the quenched-in distribution at 300 K. In the slow-quenched model the number of subcritical nuclei slightly increases with time at constant temperature with respect to the value at the beginning of the

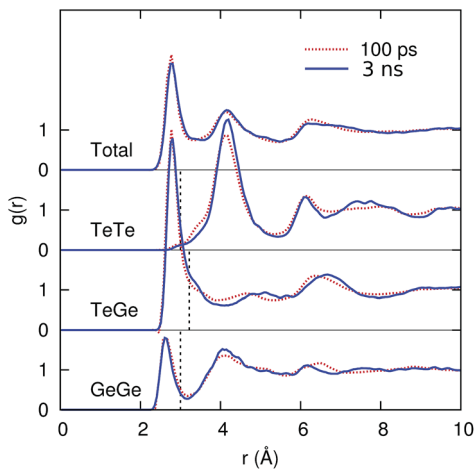

Fig. 7 Total and partial pair correlation functions of the two models of a-GeTe quenched from the melt in either 100 ps or 3 ns (see Fig. 1).

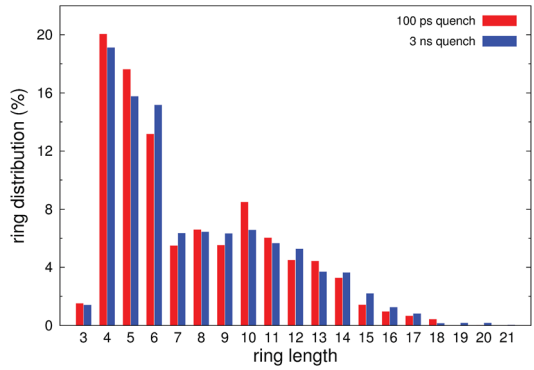

Fig. 8 Distribution of ring lengths in the slow- and fast-quenched models of a-GeTe (see Fig. 1).

simulation up to 575 K which is close to the temperature of maximum nucleation rate of 0.55 T_m found in ref. 15 from a CNT analysis of the crystallization kinetics of GST. Still, as it occurs in the fast-quenched model, a sufficiently large number of subcritical nuclei survives at the highest temperatures to promote the formation and growth of overcritical nuclei with no incubation time. In fact, the overall number of crystalline atoms increases smoothly with time at all temperatures from the beginning of the simulation as shown in Fig. 10 until interactions

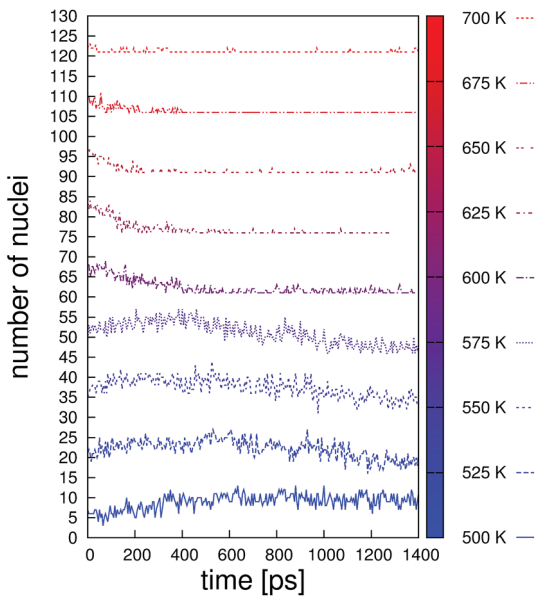

Fig. 9 The number of crystalline nuclei containing more than 8 atoms as a function of time in constant temperature simulations of the slow-quenched model of a-GeTe (see text). The evolution in time of the population of nuclei is reported at different temperatures. The curves corresponding to the different temperatures are shifted by 15 units along the ordinate axis.

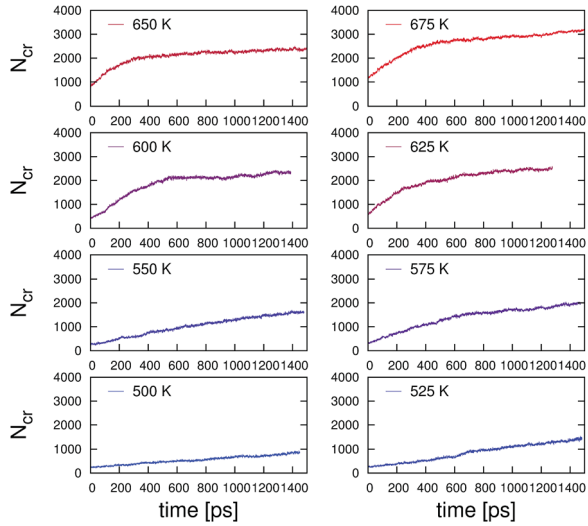

Fig. 10 Evolution with time of the number of crystalline atoms N_{cr} at different temperatures during the crystallization of the slow-quenched model of a-GeTe (see text). The model is heated from 300 K to 700 K in nine steps lasting 50 ps each. The system is then monitored for 1.4 ns at constant temperature at each step of the heating process.

among the nuclei slow down the crystallization process at the highest temperatures. We remark that, as observed in the fast-quenched model, the presence of a large population of subcritical nuclei does not lead to an overall increase in the crystal growth velocity but just to a reduction/disappearance of the incubation time.

4 Conclusions

We have reported atomistic simulations of the crystallization kinetics of a-GeTe annealed above T_g at different temperatures in the range 500–700 K. The results on the crystal growth velocity of supercritical nuclei are very similar to those obtained in our previous work[24] for the supercooled liquid quenched in steps from T_m. The process of annealing of the amorphous models allows for the formation of a large population of subcritical nuclei at the lower temperatures where the nucleation rate is large and critical nuclei are small. The fast heating protocol (50 ps for each step of 25 K temperature increase) allows the subcritical nuclei to survive at the highest temperatures at which some of them dissolve, but others grow becoming overcritical. This process leads to a disappearance of the incubation time at all temperatures in the range 550–700 K and thus up to temperatures where the crystal growth velocity is maximal and nucleation rate is low.

This outcome provides further evidence on the viability of exploiting priming effects to improve the set process in the ultra-scaled memory cell as suggested in previous work.[17,48] In ultra-scaled memories one might conceive that the whole active volume can turn into the amorphous phase. Under these conditions and in the lack of a crystal-amorphous interface, crystal nucleation might become the

rate limiting step of the set process. Variability in the set process from cell to cell is expected to exacerbate by shrinking the cell size due to the inherent stochasticity of the nucleation process. Our results show that the incubation time and thus the stochasticity of nucleation could be drastically reduced by properly designing the heating protocol in such as way that the system spent a sufficient time (actually just few tens of ps in our simulations) at lower temperatures where the nucleation rate is large. Fast annealing can then result in the population of subcritical nuclei at higher temperatures where some nuclei can grow overcritical under conditions at which the crystal growth velocity is maximal.

Conflicts of interest

There are no conflicts to declare.

Acknowledgements

This work was partially supported by the European Union Seventh Framework Program FP7/2007-2013 under Grant Agreement 310339. We acknowledge the computational resources provided by Cineca (Casalecchio di Reno, Italy) through the ISCRA program.

Notes and references

1 M. Wuttig and N. Yamada, *Nat. Mater.*, 2007, **6**, 824–832.
2 A. Pirovano, A. L. Lacaita, A. Benvenuti, F. Pellizzer and R. Bez, *IEEE Trans. Electron Devices*, 2004, **51**, 452–459.
3 A. L. Lacaita and A. Redaelli, *Microelectron. Eng.*, 2013, **109**, 351–356.
4 D. Lencer, M. Salinga and M. Wuttig, *Adv. Mater.*, 2011, **23**, 2030–2058.
5 S. Raoux, W. Welnic and D. Ielmini, *Chem. Rev.*, 2010, **110**, 240–267.
6 G. W. Burr, B. N. Kurdi, J. C. Scott, C. H. Lam, K. Gopalakrishnan and R. S. Shenoy, *IBM J. Res. Dev.*, 2008, **52**, 449–464.
7 J. Orava, A. L. Greer, B. Gholipour, D. W. Hewak and C. E. Smith, *Nat. Mater.*, 2012, **11**, 279–283.
8 B. Chen, G. H. ten Brink, G. Palasantzas and B. J. Kooi, *J. Phys. Chem. C*, 2017, **121**, 8569–8578.
9 B. Chen, D. de Wal, G. H. ten Brink, G. Palasantzas and B. J. Kooi, *Cryst. Growth Des.*, 2018, **18**, 1041–1046.
10 Y. Chen, G. Wang, L. Song, X. Shen, J. Wang, J. Huo, R. Wang, T. Xu, S. Dai and Q. Nie, *Cryst. Growth Des.*, 2017, **17**, 3687–3693.
11 N. Ciocchini, M. Cassinerio, D. Fugazza and D. Ielmini, *IEEE Trans. Electron Devices*, 2013, **60**, 3767–3774.
12 A. Sebastian, M. Le Gallo and D. Krebs, *Nat. Commun.*, 2014, **5**, 4314.
13 R. Jeyasingh, S. W. Fong, J. Lee, Z. Li, K. Chang, D. Mantegazza, M. Asheghi, K. E. Goodson and H. P. Wong, *Nano Lett.*, 2014, **14**, 3419–3426.
14 M. K. Santala, B. W. Reed, S. Raoux, T. Topuria, T. La Grange and G. H. Campbell, *Appl. Phys. Lett.*, 2013, **102**, 174105.
15 J. Orava and L. A. Greer, *Acta Mater.*, 2017, **139**, 226–235.
16 V. Weidenhof, I. Friedrich, S. Ziegler and M. Wuttig, *J. Appl. Phys.*, 2001, **89**, 3168–3176.

17 D. Loke, T. H. Lee, W. J. Wang, L. P. Shi, R. Zhao, Y. C. Yeo, T. C. Chong and S. R. Elliott, *Science*, 2012, **336**, 1566–1569.
18 J. Hegedüs and S. R. Elliott, *Nat. Mater.*, 2008, **7**, 399–405; T. H. Lee and S. R. Elliott, *Phys. Rev. Lett.*, 2011, **107**, 145702.
19 J. Kalikka, J. Akola and R. O. Jones, *Phys. Rev. B*, 2016, **94**, 134105; J. Kalikka, J. Akola, J. Larrucea and R. O. Jones, *Phys. Rev. B: Condens. Matter Mater. Phys.*, 2012, **86**, 144113.
20 I. Ronnenberg, W. Zhang, H. Eshet and R. Mazzarello, *Adv. Funct. Mater.*, 2015, **25**, 6407–6413.
21 P. S. Branicio, K. Bai, H. Ramanarayan, D. T. Wu, M. B. Sullivan and D. J. Srolovitz, *Phys. Rev. Mater.*, 2018, **2**, 043401.
22 J. Kalikka, J. Akola and R. O. Jones, *Phys. Rev. B: Condens. Matter Mater. Phys.*, 2014, **90**, 184109.
23 F. Rao, K. Ding, Y. Zhou, Y. Zheng, M. Xia, S. Lv, Z. Song, S. Feng, I. Ronneberger, R. Mazzarello, W. Zhang and E. Ma, *Science*, 2017, **358**, 1423–1427.
24 G. C. Sosso, G. Miceli, S. Caravati, J. Behler and M. Bernasconi, *J. Phys. Chem. Lett.*, 2013, **4**, 4241–4246.
25 G. C. Sosso, M. Salvalaglio, J. Behler, M. Bernasconi and M. Parrinello, *J. Phys. Chem. C*, 2015, **119**, 6428–6434.
26 G. C. Sosso, G. Miceli, S. Caravati, J. Behler and M. Bernasconi, *Phys. Rev. B: Condens. Matter Mater. Phys.*, 2012, **85**, 174103.
27 S. Gabardi, E. Baldi, E. Bosoni, D. Campi, S. Caravati, G. C. Sosso, J. Behler and M. Bernasconi, *J. Phys. Chem. C*, 2017, **121**, 23827–23838.
28 K. F. Kelton and M. C. Weinberg, *J. Non-Cryst. Solids*, 1994, **180**, 17–24.
29 J. Behler and M. Parrinello, *Phys. Rev. Lett.*, 2007, **98**, 146401; J. Behler, *Angew. Chem., Int. Ed.*, 2017, **56**, 12828.
30 J. P. Perdew, K. Burke and M. Ernzerhof, *Phys. Rev. Lett.*, 1996, **77**, 3865–3868.
31 P. Giannozzi, S. Baroni, N. Bonini, M. Calandra, R. Car, C. Cavazzoni, D. Ceresoli, G. L. Chiarotti, M. Cococcioni, I. Dabo, A. D. Corso, S. de Gironcoli, S. Fabris, G. Fratesi, R. Gebauer, U. Gerstmann, C. Gougoussis, A. Kokalj, M. Lazzeri, L. Martin-Samos, N. Marzari, F. Mauri, R. Mazzarello, S. Paolini, A. Pasquarello, L. Paulatto, C. Sbraccia, S. Scandolo, G. Sclauzero, A. P. Seitsonen, A. Smogunov, P. Umari and R. M. Wentzcovitch, *J. Phys.: Condens. Matter*, 2009, **21**, 395502; www.quantum-espresso.org.
32 G. C. Sosso, J. Behler and M. Bernasconi, *Phys. Status Solidi B*, 2012, **249**, 1880–1885.
33 G. C. Sosso, D. Donadio, S. Caravati, J. Behler and M. Bernasconi, *Phys. Rev. B*, 2012, **86**, 104301.
34 G. C. Sosso, J. Colombo, E. Del Gado, J. Behler and M. Bernasconi, *J. Phys. Chem. B*, 2014, **118**, 13621–13628.
35 S. Gabardi, S. Caravati, G. C. Sosso, J. Behler and M. Bernasconi, *Phys. Rev. B*, 2015, **92**, 054201.
36 D. Campi, D. Donadio, G. C. Sosso, J. Behler and M. Bernasconi, *J. Appl. Phys.*, 2015, **117**, 015304.
37 W. Klemm and G. Frischmuth, *Z. Anorg. Chem.*, 1934, **218**, 249–251.
38 J. Behler, *RuNNer: A Neural Network Code for High-Dimensional Potential-Energy Surfaces*, Institut für Physikalische Chemie, Universität Göttingen: Göttingen, Germany, 2012.

39 W. Smith and T. R. Forester, *J. Mol. Graphics*, 1996, **14**, 136–141.
40 G. Bussi, D. Donadio and M. Parrinello, *J. Chem. Phys.*, 2007, **126**, 014101.
41 G. E. Ghezzi, J. Y. Raty, S. Maitrejean, A. Roule, E. Elkaim and F. Hippert, *Appl. Phys. Lett.*, 2011, **99**, 151906.
42 P. J. Steinhardt, D. R. Nelson and M. Ronchetti, *Phys. Rev. B*, 1983, **28**, 784–805.
43 J. S. van Duijneveldt and D. Frenkel, *J. Chem. Phys.*, 1992, **96**, 4655–4668.
44 G. C. Sosso, J. Behler and M. Bernasconi, *Phys. Status Solidi A*, 2016, **213**, 329–334.
45 H. Weber, M. Schumacher, P. Jovari, P. Tsuchiya, W. Skrotzki, R. Mazzarello and I. Kaban, *Phys. Rev. B*, 2017, **96**, 054204.
46 K. Lee, E. D. Murray, L. Kong, B. I. Lundqvist and D. C. Langreth, *Phys. Rev. B*, 2010, **82**, 081101.
47 K. F. Kelton, A. L. Greer and C. V. Thompson, *J. Chem. Phys.*, 1983, **79**, 6261–6276.
48 T. H. Lee, D. Loke, K.-J. Huang, W.-J. Wang and S. R. Elliott, *Adv. Mater.*, 2014, **26**, 7493–7498.
49 S. Caravati, G. C. Sosso and M. Bernasconi, Functional Properties of Phase Change Materials from Atomistic Simulations, in *Molecular Dynamics Simulations of Disordered Materials. From Network Glasses to Phase-Change Memory Alloys*, ed. C. Massobrio, J. Du, M. Bernasconi and P. S. Salmon, Springer Series in Materials Science, Springer, Berlin, 2015, vol. 215, pp. 415–440, ISBN: 978-3-319-15674-3 (Print) 978-3-319-15675-0.
50 D. S. Franzblau, *Phys. Rev. B*, 1991, **44**, 4925–4930.